J. Fluid Mech. (1988), *vol.* 194, *pp.* 133–151
Printed in Great Britain

The turbulent layer in the water at an air–water interface

By TAK KEE CHEUNG† AND ROBERT L. STREET‡

† UGAR Scientist at Naval Environmental Prediction Research Facility, Monterey, CA 93943-5006, USA

‡ Environmental Fluid Mechanics Laboratory, Department of Civil Engineering, Stanford University, Stanford, CA 94305, USA

(Received 26 December 1985 and in revised form 30 November 1987)

The velocity fields beneath an air–water interface have been determined in a laboratory facility for the cases of wind-generated waves, with wind speeds ranging from 1.5 to 13.1 m/s, and of wind-ruffled mechanically generated waves of about 22 mm amplitude and 1 Hz frequency, with wind speeds ranging from 1.7 to 6.2 m/s. The velocity was measured in a fixed frame of reference with a two-component, laser-Doppler anemometer. It was possible to determine the lengthscales and evaluate the behaviour of the mean, wave-related and turbulent components of the flows. The waves affect the mean flows, even though the profiles remain essentially logarithmic and the wave field conforms generally with the results of linear theory. In the wind-wave cases the turbulent quantities behave similarly to those in flows over flat plates. They have different trends in the mechanical-wave cases, suggesting a coupling between waves and turbulence. Finally, measured values of the mean wave-induced shear stress were negative, leading to an energy transfer from the waves to the mean flow.

1. Introduction

When wind blows over water waves, energy which is transferred from the wind is distributed in the water near the interface among the mean drift current, turbulence, and wave motion. How does this distribution change with depth? How do the turbulent and wave quantities behave near the interface? Questions such as these are perhaps best answered by performing laboratory experiments.

From the work of Shemdin (1972), Wu (1975) and McLeish & Putland (1975) it is known that the current immediately below the water surface varies linearly with depth and the current near, but not immediately below, the water surface follows a logarithmic velocity distribution. Dobroklonskiy & Lesnikov (1975) reported logarithmic mean drift-velocity profiles and that the total Reynolds stress originated from two sources: a wave source and a turbulent source. Howe *et al.* (1982) reported laboratory measurements of velocity and temperature fields on both sides of a wind-driven air–water interface. The mean velocity profiles, both in the air and in the water, were logarithmic. They separated wave and turbulent motions and showed that in the water surface layer the velocity fluctuations due to the wave-related motion were of the same order as the purely turbulent motions [cf. Goossens, van Pagee & Tessel (1982) and Lin & Gad-el-Hak (1984)].

Bliven, Huang & Long (1984) conducted a series of laboratory experiments to measure the velocity field below surface gravity waves. Their study showed the existence of a Reynolds stress which increased as the wave steepness increased and

decayed exponentially with depth. Turbulent energy also followed the same trends. The ratio of the exponential decay rate for turbulent energy to wave-particle velocity decay rate was less than unity, which indicates that the turbulent-energy penetration depth is on the order of the wavelength rather than the wave height as suggested by Donelan (1978).

Field measurements of water velocity under wind waves were made by Bowden & White (1966), Shonting (1964, 1967, 1968, 1970), Simpson (1969), Yefimov & Khristoforov (1969, 1971), Taira (1971), Thornton & Krapohl (1974) and Cavaleri, Ewing & Smith (1978). Most showed general agreement with linear theory; however, Shonting, Yefimov & Kristoforov and Cavaleri *et al.* found vertical and horizontal velocities not in quadrature, thus indicating the existence of a downward momentum flux.

It has been suggested also that the orbital motion of waves in the water layer has little effect on turbulent transport (Kondo 1976; Jones & Kenney 1977). However, the experiments of Shonting (1967) and Yefimov & Kristoforov (1969) showed otherwise. Howe *et al.* (1982) reported that near, but not immediately below, the interface the wave-related motions were of the same order as the purely turbulent motions, and mean velocity profiles deviated from a $1/\kappa$ slope ($\kappa = 0.4$) when waves were present. Consequently, it is quite possible that organized wave motion strongly influences transport in the zone immediately below the interface.

2. The experiments

A series of experiments were undertaken in a laboratory channel to answer some of the questions raised above. Our objectives were to obtain mean and turbulent velocity data in the water layer beneath both wind-generated and wind-ruffled mechanically generated water waves, to find the similarities and differences between the results for these cases, and to compare the measured quantities with existing data and theoretical models. The measurements were made in the Stanford Wind, Water-Wave Research Facility (Cheung 1984; Hsu, Hsu & Street 1981; Bole & Hsu 1969) at a single fetch of 13 m from the inlet of the channel. The air free-stream velocities for the wind-generated-wave runs ranged from 1.5 to 13.1 m/s; for wind-ruffled mechanically generated waves, wind velocities ranged from 1.7 to 6.2 m/s. The amplitude a of about 22 mm and frequency of 1 Hz for the mechanically generated waves were chosen so that the waves were of deep-water type in the facility and small-amplitude theory was applicable. The present results include mean, wave-induced and turbulent quantities measured in the water beneath the interface. The characteristic scales of the various cases are summarized in table 1. The flow was turbulent (cf. Tennekes & Lumley 1972, pp. 1–3) even at the lowest wind speeds.

A detailed description of the present experimental set-up, qualification tests for instrumentation, determination of uncertainties, etc., can be found in Cheung (1984). The channel used for the experiments is 1.9 m high by 0.9 m wide and 35 m long with a 22 m long glass test section. For the current set of experiments, the water depth in the channel was about 1 m, leaving about 1 m for the vertical depth of the air flow. The channel includes a mechanical wave-generating plate and a dissipating beach whose reflection coefficient for waves at a frequency of 1 Hz is less than 5%. A fan draws air through the test section.

The air velocity was determined by use of a Pitot-static tube and water-surface elevation by use of capacitance wave-height gauges. Two gauges were used to resolve the various components in the mechanically generated wave cases, but only one in

u_∞ (m/s) ~3%†	u_S (mm/s) 10%	δ (mm) 10%	u_* (mm/s) 10%	$(\overline{\tilde{u}_0^2})^{\frac{1}{2}}$ (mm/s) or 2%	$2\pi f_D \hat{\eta}_S/\sqrt{2}$ (mm/s) 2%	y_η (mm) 10%	$1/k$ (mm) 2%	a (mm) 2%	f_D (Hz) <1%
				Case I (wind waves)					
1.5	40	141	2.10	0.29	—	—	—	—	—
2.6	70	310	3.40	4.44	—	—	—	—	6.1
3.2	70	348	4.94	38.26	—	9.3	—	—	5.2
4.7	93	264	7.20	76.67	—	19.9	—	—	3.5
6.7	137	249	11.30	108.34	—	32.6	—	—	2.7
9.9	204	354	17.50	139.84	—	45.1	—	—	2.4
13.1	270	298	27.50	194.06	—	58.2	—	—	2.0
				Case II (mechanical waves)					
1.7	24	99	2.20	—	93.61	—	248	21.1	1.0
2.5	41	102	3.35	—	97.08	—	248	21.9	1.0
4.1	62	168	5.35	—	98.23	—	248	22.1	1.0
6.2	108	171	9.23	—	92.68	—	248	20.9	1.0

† Percentage values show uncertainty of data and scales

TABLE 1. Characteristic scales

the wind-wave cases. A two-component laser-Doppler-anemometer (LDA) system was used in the forward-scatter mode to determine the horizontal (u) and vertical (v) components of the velocity in the water. The Lagrangian surface drift was determined during each experiment by a series of measurements of the time required for paper punchings to travel a fixed distance in the channel. Time was allowed for de-aeration of the channel water and for experimental conditions to reach equilibrium. Corrections were made for set-up of the water surface and for water loss due to evaporation during each test. To ensure that the deductions made from the experimental data were significant, Nth-order uncertainty intervals as defined by Moffat (1981) were calculated for important variables by using the procedure described by Kline & McClintock (1953) (see table 1).

The data acquisition system described by Takeuchi & Mogel (1975) was used. The sampling frequency was 100 Hz for the wind-wave cases and 200 Hz for all others. Data were sampled at each depth for 10.24 min, despite the difference in sampling rate. For mechanical-wave cases, this record length allowed resolution of the anticipated lowest frequency component and accommodated more than 614 periods of the 1 Hz generated wave, sufficient for accurate phase averaging.

Following Benilov, Kouznetsov & Panin (1974), we decomposed any flow variable $f(\boldsymbol{x}, t)$, such as velocity, into three components:

$$f(\boldsymbol{x}, t) = \bar{f}(\boldsymbol{x}) + \tilde{f}(\boldsymbol{x}, t) + f'(\boldsymbol{x}, t), \tag{1}$$

where $\bar{f}(\boldsymbol{x})$ is the time-averaged or mean value of $f(\boldsymbol{x}, t)$, $\tilde{f}(\boldsymbol{x}, t)$ is the main wave-induced component, $f'(\boldsymbol{x}, t)$ is the fluctuating component, and $\boldsymbol{x}$ is the Cartesian coordinate vector (x, y, z), with x the streamwise distance (or fetch) measured with respect to the air inlet, y the vertical distance (positive upwards) measured with respect to the still-water level, and z the spanwise distance measured with respect to the centreline of the test facility. We make a clear distinction here regarding waves. In the case of wind waves (Case I), $\tilde{f}$ includes all the wave-induced motion. However, in Case II where mechanically generated waves are present, we let $\tilde{f}$ represent effects of these waves and let $f' = f_R + f_T$, where f_R represents quantities induced by wind-

generated ripples and f_T represents turbulent quantities. It follows, then, that in Case I, $f' = f_T$.

The time average is defined as

$$\bar{f}(\boldsymbol{x}) = \lim_{T\to\infty} \frac{1}{T} \int_0^T f(\boldsymbol{x}, t)\, \mathrm{d}t. \tag{2}$$

It is also assumed that both $\tilde{f}$ and f' have zero means, i.e. $\bar{\tilde{f}} = 0$ and $\overline{f'} = 0$. The statistical properties of $\tilde{f}$ and f' are found by the wave-separation method outlined below.

2.1. *Case I: wind waves – wave-separation method*

In order to isolate the wave component of a flow variable, the wave-induced component $\tilde{f}(\boldsymbol{x}, t)$ is assumed to be statistically coherent with the surface displacement $\eta(\boldsymbol{r}, t)$. Then,

$$\tilde{f}(\boldsymbol{x}, t) = \mathrm{L}\eta(\boldsymbol{r}, t)$$

and

$$\overline{\tilde{f}\bar{f}} = 0, \quad \overline{\tilde{f}f'} = 0, \quad \overline{\bar{f}f'} = 0,$$

where L is some linear operator, $\boldsymbol{r} = (x, y)$ is a horizontal vector at the interface, and η is composed of wave components only, i.e. $\eta = \tilde{\eta}$ and $\bar{\eta} \equiv \eta' \equiv 0$. This approach has been previously adopted by Benilov *et al.* (1974), Howe *et al.* (1981, 1982), Kitaigorodskii *et al.* (1983) and Bliven *et al.* (1984). Howe *et al.* (1981) showed that the second moments of $\tilde{f}$ and f' can be obtained without reconstructing realizations of $\tilde{f}$ and f'. Howe *et al.* (1982) noted, however, that turbulent components that are correlated with the wave will be incorporated in and computed as a part of the equivalent wave component.

2.2. *Case II: wind-ruffled, mechanically generated waves – phase-averaging method*

One can decompose each flow variable into three components in a manner similar to that used for the wind-wave case. The time average of f was defined in (2). To separate out the *periodic* component $\tilde{f}$, we use a phase average:

$$\langle f(\boldsymbol{x}, t)\rangle = \lim_{N\to\infty} \frac{1}{N} \sum_{n=0}^{N-1} f(\boldsymbol{x}, t + n\tau), \tag{3}$$

where τ is the period of the mechanically generated wave. In practice, N is always finite but large.

Because $f' = f_R + f_T$ is not correlated with the mechanical wave, the phase average of f contains only the mean and the periodic components, i.e.

$$\langle f(\boldsymbol{x}, t)\rangle = \bar{f}(\boldsymbol{x}) + \tilde{f}(\boldsymbol{x}, t)$$

and so

$$\langle \overline{f(\boldsymbol{x}, t)}\rangle = \bar{f}(\boldsymbol{x}), \quad \tilde{f}(\boldsymbol{x}, t) = \langle f(\boldsymbol{x}, t)\rangle - \bar{f}(x), \quad f'(\boldsymbol{x}, t) = f(\boldsymbol{x}, t) - \langle f(\boldsymbol{x}, t)\rangle$$

(Hussain & Reynolds 1970). However, f' does include the effects of both the wind-generated ripples (in f_R) and the turbulence (in f_T).

2.3. *Analysis*

The wave-separation method was used in Case I (wind waves) experiments to deduce the means and second moments of all quantities. Two steps were necessary in analysing the data, namely, establishing the time mean for each channel of data in

an experiment and using the wave-separation program to find the wave-induced and turbulent quantities.

For Case II (mechanical waves), the time mean for each channel of data was calculated first. Second, the wave period of the reference wave-height signal was determined (Cheung 1984) and the phase averages were calculated. Third, the mean turbulent stresses ($\overline{u_i' u_j'}$), mean wave-induced stresses ($\overline{\tilde{u}_i \tilde{u}_j}$), and other wave-related quantities $\widetilde{u_i' u_j'}$ were calculated and the amplitude and phase of $\tilde{u}$, $\tilde{v}$, $\widetilde{u_i' u_j'}$, and $\tilde{\eta}$ were found by a cross-spectral method and a cosine-fitting technique (Cheung 1984). Finally, using the phase-averaged results, we resampled the original data sets in exactly the same manner as used in the phase-averaging process, but the phase-averaged result was subtracted point by point and new data sets for $f' = f_R + f_T$ were constructed for further analysis (note $\eta = \tilde{\eta} + \eta_R$, where $\tilde{\eta}$ is the phase-averaged mechanical wave and η_R represents the wind-generated ripples).

3. Case I: wind waves

The mean Eulerian surface drift ($\bar{u}_S$) at the location of the wave-height gauge is

$$\bar{u}_S = \bar{u}_{SL} - \bar{u}_{Stokes},$$

where $\bar{u}_{SL}$ is the mean Lagrangian surface drift and $\bar{u}_{Stokes}$ is the mass transport velocity (Phillips 1977, p. 44) deduced from the surface-elevation spectrum according to the method of Bye (1967) (see Cheung 1984). The Eulerian surface drift is about 2% of the free-stream velocity and the Lagrangian drift about 3% of the free-stream wind speed. These results are in agreement with Wu (1968) and Phillips & Banner (1974).

Mean velocity profiles are plotted in wall coordinates in figure 1. Here, we use a velocity-defect representation of the data, viz. $u^+ = (\bar{u}_S - \bar{u})/u_*$ and $y^+ = yu_*/\nu_w$, where u_* is the friction velocity and ν_w is the kinematic viscosity of water. Values of u_*^2 were obtained by extrapolating to the interface a linear least-squares fit (with depth) of the direct turbulent shear stress ($-\overline{u'v'}$) measurements. For the complex flow in our experimental facility, in which the turbulent boundary layer overlies a slow return flow, we may define a vertical lengthscale δ as the depth at which the turbulent shear stress vanishes (the δ are determined from the same least-squares-fit lines used in deducing u_*^2). This definition of δ has the equivalent physical meaning of a thickness for a turbulent boundary layer (Goossens *et al.* 1982); at the fetch (13 m) of the present measurements the boundary layer is well developed and changes with fetch are small.

The visual appearance of the water surface varied from smooth to rough for the range of wind speeds used in the experiments. Also plotted in figure 1 for reference are the universal law of the wall for a turbulent flow with zero pressure gradient over smooth walls and a line that demarks the beginning of the fully rough regime (see Schlichting 1979, pp. 616–623). The velocity profile for the lowest wind speed clusters around the smooth-wall relationship and as wind speed increases, the usual shift associated with the apparent increase in surface roughness occurs. In addition, for the two lowest wind speeds, the profiles extend to follow the $u^+ = -y^+$ line, which suggests the existence of a viscous sublayer. Hence, the velocity and lengthscales appropriate for flows over solid surfaces are also applicable for the water boundary layer at low wind speeds. However, the surface drift plays a significant role because $\bar{u}_S$ is related to u_* (cf. Wu 1975).

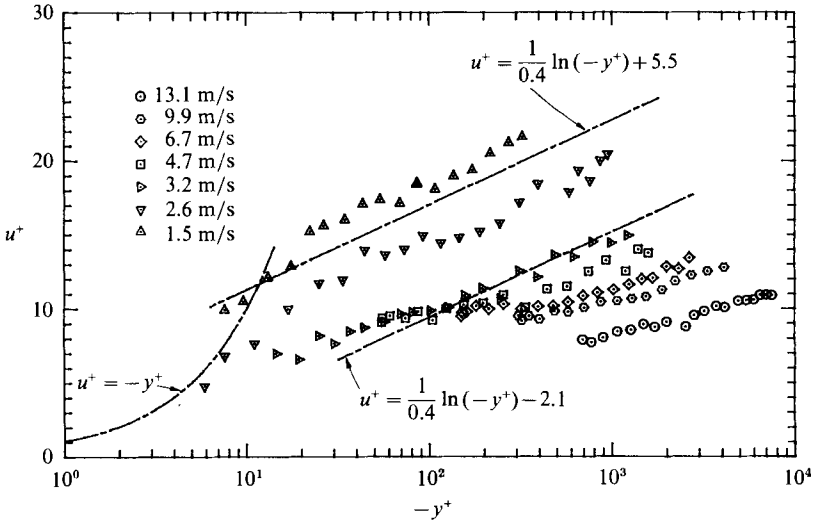

FIGURE 1. Mean horizontal velocity-defect profile in law-of-the-wall coordinates: wind waves (case I).

For wind speeds higher than 3.2 m/s, all the profiles lie below the relationship representing the start of the fully rough flow regime. In addition, the mean velocity profiles remain logarithmic, although waves were present and significant at the interface. However, the slopes of some of the profiles are different from those at low wind speeds. Furthermore, there is an apparent change of slope in profiles at wind speeds of 3.2, 4.7 and 6.7 m/s. There is no change of slope in the profile at the two highest wind speeds, but the slope of the profile is clearly different from that in the low-wind-speed experiments. Similar behaviour was reported by Howe *et al.* (1982). A possible explanation is discussed in §5.

For all wind speeds, with the exception of the highest, the mean vertical velocity profiles (not plotted here) fall within a band of ± 3 mm/s about zero. In addition, the mean vertical velocity gradient (with depth) is very close to zero at all depths and at all wind speeds.

The root-mean-square (r.m.s.) velocity fluctuation $[(\overline{u'^2})^{\frac{1}{2}}, (\overline{v'^2})^{\frac{1}{2}}]$ profiles are plotted in non-dimensional form in figures 2 and 3. The $u'_{\rm rms}$ profiles for *all* wind speeds collapse within a narrow band when normalized by u_* and δ. The $v'_{\rm rms}$ profiles for wind speeds higher than 3 m/s also coalesce into a band when normalized by the same parameters. Thus, u_* and δ are the appropriate velocity and lengthscales relating turbulent velocity fluctuations and turbulence decay with depth (see table 1 for their values). The fact that δ is the appropriate lengthscale is intuitively obvious, because the largest turbulent eddy is probably on the order of the thickness of the turbulent boundary layer. Similarly, because u_* is derived from the turbulent shear stress, which is directly responsible for turbulence generation, the turbulent intensities should scale with u_*. Also plotted in the figures are the data of Klebanoff (1955) for a turbulent boundary layer with zero pressure gradient. The $u'_{\rm rms}$ profiles follow this reference data reasonably well, but generally lie above it. The $v'_{\rm rms}$ profiles also group around the reference data except for the lower wind-speed experiments. It is clear that anisotropy exists between $u'_{\rm rms}$ and $v'_{\rm rms}$ within the boundary layer. In addition, the degree of anisotropy increases towards the interface. On the other

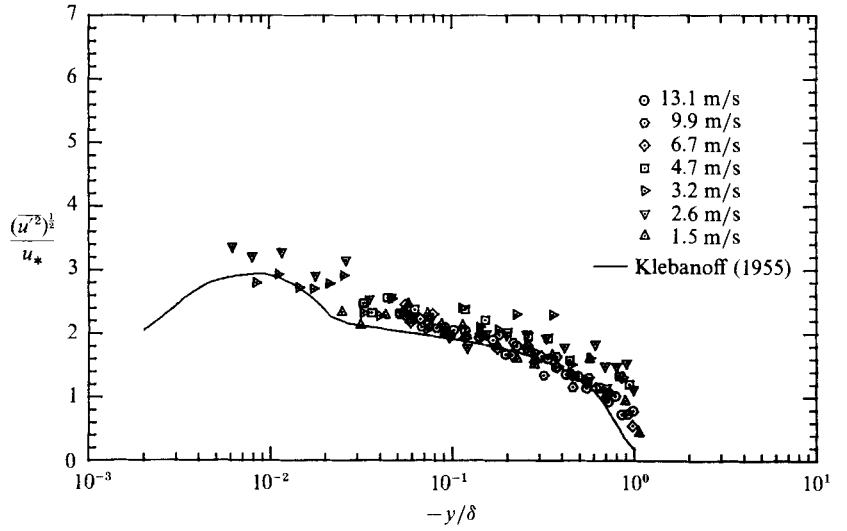

FIGURE 2. $(\overline{u'^2})^{\frac{1}{2}}/u_*$ versus $-y/\delta$: wind waves (case I).

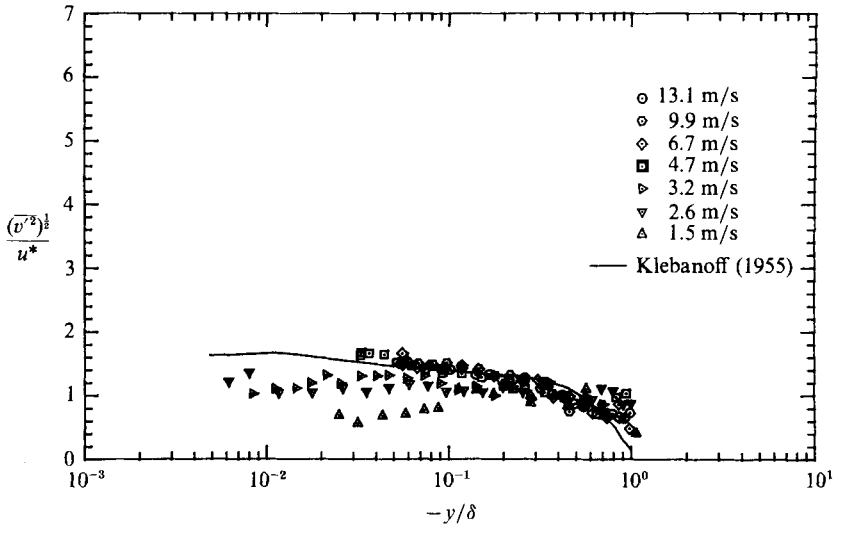

FIGURE 3. $(\overline{v'^2})^{\frac{1}{2}}/u_*$ versus $-y/\delta$: wind waves (case I).

hand, turbulent fluctuations decrease and become more isotropic near the edge of the boundary layer.

Figure 4 shows some typical mean wave-induced shear-stress ($-\overline{\tilde{u}\tilde{v}}$) profiles. The wave-induced shear stress is *negative* very close to the interface and decays very rapidly with depth. If one defines a penetration depth for the wave-induced shear stress as the depth at which the wave-induced shear stress vanishes, then the penetration depth increases with wind speed, but is at most equal to 0.2δ for the highest wind speed, and is considerably less for lower-wind-speed experiments. The wave-induced shear stress is of the order of u_*^2 near the surface and comprises most of the total shear stress within that region. However, the turbulent shear stress seems to be the dominant component over most parts of the boundary layer.

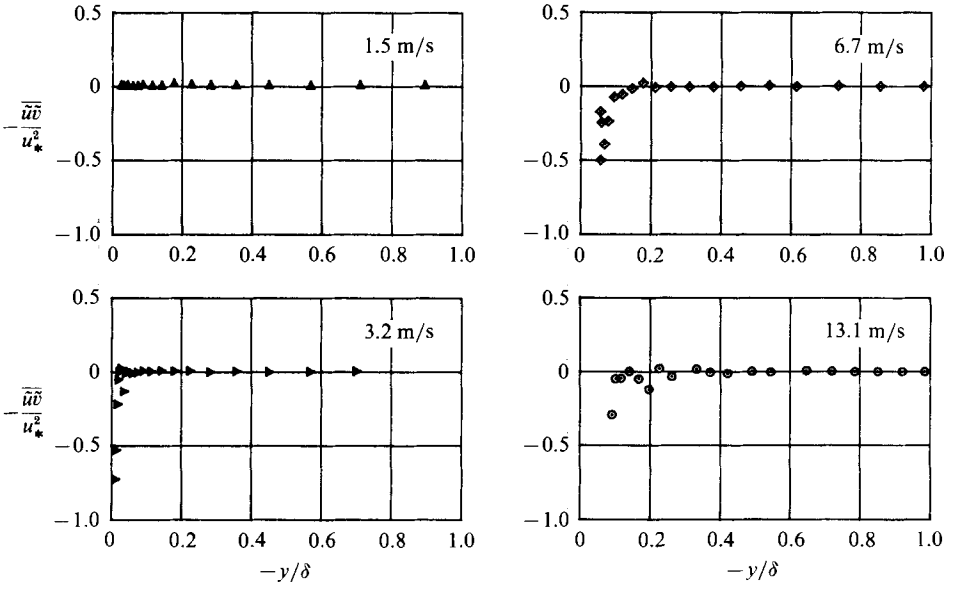

FIGURE 4. $-\overline{\tilde{u}\tilde{v}}/u_*^2$ versus $-y/\delta$: wind waves (case I).

The relevant scales for the mean and turbulent parts of the flows are similar to those for wall-bounded shear flows. However, the wind-generated waves introduce additional velocity and lengthscales. Profiles (not shown here) of the r.m.s. wave-induced velocities $(\overline{\tilde{u}^2})^{\frac{1}{2}}$ and $(\overline{\tilde{v}^2})^{\frac{1}{2}}$ are nicely collapsed by normalizing the velocities by the r.m.s. surface orbital velocity $(\overline{\tilde{u}_0^2})^{\frac{1}{2}}$, computed from the wave-height signal, and normalizing the depth by a wave-decay depth y_η (see Cheung 1984). Here, $\overline{\tilde{u}_0^2}$ is given, according to linear theory, by

$$\overline{\tilde{u}_0^2} = \int_0^{f_c} (2\pi f)^2 S_{\eta\eta}(f)\,\mathrm{d}f, \tag{4}$$

where $S_{\eta\eta}(f)$ is the one-sided power spectrum of the wave-height signal η and f_c ($=10$ Hz) is the assumed upper frequency limit for gravity waves. Then, y_η is the depth at which the integrated-surface orbital amplitude decays by a factor of e^{-1} (Howe *et al.* 1982). When the r.m.s. wave-induced velocity profiles are normalized, for example, by u_* and δ, the profiles do not collapse, thus confirming that $(\overline{\tilde{u}_0^2})^{\frac{1}{2}}$ and y_η are appropriate characteristic scales for the wave-induced quantities.

4. Case II: mechanical waves

The main distinction between this case and the wind-wave case (Case I) is the presence of the 1 Hz mechanically generated waves. In Case I, the waves were generated solely by the wind. Here, the dominant waves were generated by mechanical means, then acted upon by the turbulent air flow. Small wavelets (ripples) are generated by the wind. The ripples randomly distorted the mechanically generated wave profile from that of an almost pure sinusoid. The mean drift velocities, both Lagrangian and Eulerian, for this set of experiments were consistently lower than those for wind-wave runs at equivalent wind speeds. It is believed that the mechanical wave provides some sheltering effects from the wind

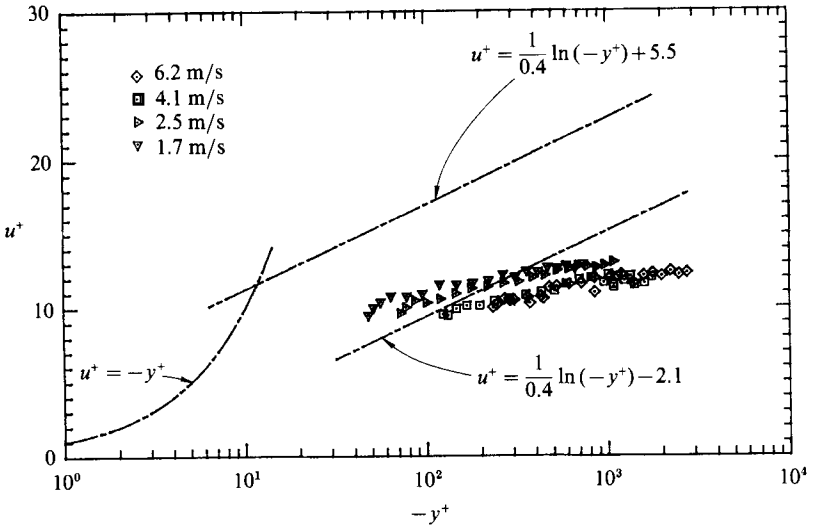

FIGURE 5. Mean horizontal velocity-defect profiles in law-of-the-wall coordinates: mechanical waves (case II).

along the wave trough (cf. Bole & Hsu 1969), thus leading to a lower mean drift velocity.

The velocity-defect profiles in wall coordinates are plotted in figure 5, together with the reference relationships cited previously for smooth- and rough-wall flows for comparison. Because the mechanically generated wave has an amplitude of about 22 mm, the closest measuring point is at least 22 mm from the mean water level. Consequently, the first data points lie at considerably greater y^+ than in Case I (figure 1).

The mean velocity profiles are logarithmic (figure 5). Although the slopes of the profiles are not 2.5 ($=1/0.4$), they are practically identical to those in the high-wind-speed wind-wave experiments. It is reasonable, then, to conclude that the significant velocity scales are u_* and $\bar{u}_S$ (as before) and that the velocity-defect distribution varies with $-\kappa y$. Of course, the value of κ is not equal to that usually taken by the von Kármán constant (0.4) because the velocity profiles have a different slope. However, κ is of the same order as 0.4. At $u_\infty = 1.7$ and 2.5 m/s, the profiles deviate from the logarithmic regions as the interface is approached (i.e. small $-y^+$). The data near this region behave as if the profiles were in a viscous sublayer, but at a higher $-y^+$ than the expected, $-y^+ \sim 11$. This results from the water motion following the surface motion of the mechanical wave (see Cheung 1984). The defining lengthscale for the mean flow boundary layer remains δ which defines the zone over which there is a substantial mean velocity gradient. The growth of the boundary layer is related, of course, to another lengthscale – the fetch – but that relationship is not explored here.

The gradient of mean vertical velocity with depth is very much smaller than the gradient of the mean horizontal velocity. The mean vertical velocities (not shown) are within ± 2 mm/s about zero for the two low-wind-speed experiments, and ± 6 mm/s at higher wind speeds.

As noted above, the data sets $f' = f_R + f_T$ were constructed by phase averaging, but now f' represents *both* the wind-generated ripple-induced (f_R) and the turbulent motions (f_T). As an example, the u'_{rms} profiles are presented in figure 6 using the same

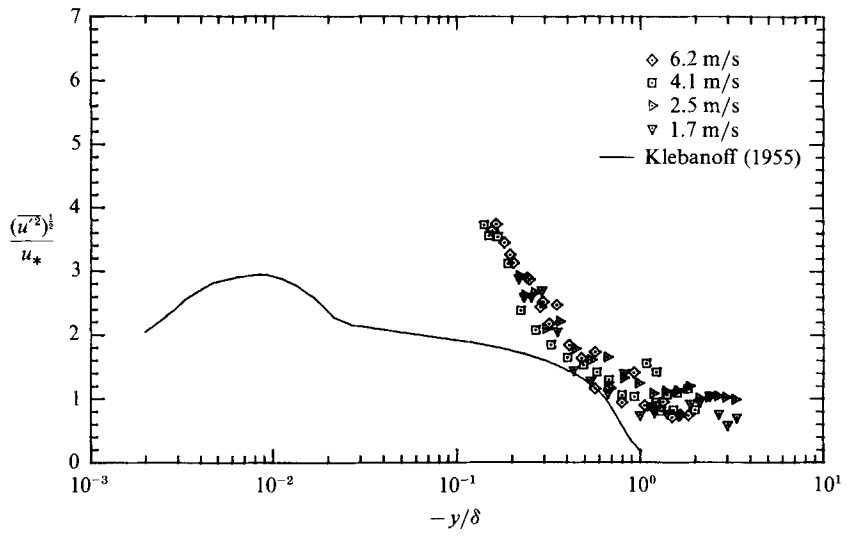

FIGURE 6. $(\overline{u'^2})^{\frac{1}{2}}/u_*$ versus $-y/\delta$, where $u' = u_R + u_T$: mechanical waves (case II).

scales as those for wind-wave experiments. These data behave very differently from those in the wind-wave case (cf. the data of Klebanoff 1955). (The v'_{rms} profiles, which are not shown, have a similar shape and relation to the Klebanoff data.) The normalized u'_{rms} and v'_{rms} have values near unity for $-y/\delta > 1$, then increase rapidly towards the interface. In addition, there is no longer anisotropy between u'_{rms} and v'_{rms}, in contrast to the anisotropy observed for the purely turbulent fluctuations beneath wind-generated waves in Case I. The data collapse for various wind speeds is good. Therefore, u_* and δ remain appropriate scaling parameters for the fluctuating part of the flow field.

The turbulence level is low at a depth near δ. However, the wave quantities are still significant in this region because the dominant wave is long. This is quite different from the wind-wave case where *both* the turbulent and wave quantities are small in the outer layer.

Now let us focus on the difference in the definition of the fluctuating quantity η' between Case I and Case II. In Case I, even though the frequency of some of the surface waves may not be the same as that of the dominant wave, they are still classified as surface waves. In the present case, any non-periodic components, i.e. components that do not have a fixed-phase relationship with the mechanically generated wave, are considered as fluctuating components. For example, the wind-generated ripples are considered as the fluctuating component of η. The ripples, of course, contribute to the u'_{rms} or v'_{rms}. Although η' has a 'wave-like' nature, the u'_{rms} and v'_{rms} do not scale with any attributes of the dominant wave, because the ripple-induced velocity is only a small component of u'_{rms} or v'_{rms} (see §6).

Although we do not plot it here, we observe that, similar to the wind-wave experiments, the mean wave-induced $(-\overline{\tilde{u}\tilde{v}})$ shear stress is negative. Here, the mean wave-induced shear stress results from motions induced by the 1 Hz mechanically generated waves. Although surface ripples are present, they are not educed by the phase-averaging process. Hence, the ripples do not contribute to $-\overline{\tilde{u}\tilde{v}}$ according to our decomposition scheme. Even at the highest wind speed, the mean wave-induced shear stress remains the dominant component in the total mean shear stress within

the region δ where turbulence is active. In physical units, there is a definite increase in mean wave-induced shear stress with wind speed.

It is relatively straightforward to characterize the mechanically generated wavetrain because its frequency and mean amplitude are well defined. For a *monochromatic* wave, the power spectrum

$$S_{\eta\eta}(f) = \tfrac{1}{2}\hat{\eta}_S^2\,\delta(f-f_D), \tag{5}$$

where $\delta(f)$ is the Dirac delta function, f_D is the frequency of the wave, and $\hat{\eta}_S$ its amplitude. The wave decay depth y_η then becomes $1/k$ where $k = 2\pi/L_w$ and $L_w = 1.56$ m is the wavelength of the mechanical wave. Substituting the above expression for $S_{\eta\eta}(f)$ into (4) gives an estimate of the mechanical-wave velocity scale $(\overline{\tilde{u}_0^2})^{\frac{1}{2}} = 2\pi f_D\,\hat{\eta}_S/\sqrt{2}$, where $f_D = 1$ Hz and $\hat{\eta}_S$ is the mean amplitude of the 1 Hz component of the water-wave spectra.

The periodic velocities $(\tilde{u}, \tilde{v})$ are nearly sinusoidal with the same frequency as that of the progressive water waves. The amplitudes $(\hat{u}, \hat{v})$ and the phase angles $(\theta_{\tilde{u}}, \theta_{\tilde{v}})$, with respect to $\tilde{\eta}$, of the first harmonic of these velocities were obtained by the spectral technique documented in Hsu *et al.* (1981). The total harmonic energy content of $\tilde{u}$ or $\tilde{v}$ is at most 2.6%. Therefore, it is sufficient to consider the amplitude and the phase of the periodic velocity only at the excitation frequency. The following observations hold *irrespective* of wind speed and depth:

(i) The amplitude distribution of $\hat{u}$ and $\hat{v}$ shows an exponential decay with depth, with normalized $\hat{v}$ being systematically larger than $\hat{u}$.

(ii) The phase lag of $\hat{u}$ with respect to the phase of $\hat{\eta}_S$ is very close to zero, but not exactly so. The phase lag varies between $-3°$ and $+2°$ about 0 for all data points.

(iii) The phase difference, $\theta_{\tilde{u}} - \theta_{\tilde{v}}$, is always slightly less than 90°. Specifically, the phase difference remains relatively constant at about 89°, except at $u_\infty = 6.2$ m/s where the phase difference decreases to about 86°.

Since the wave-induced motion can be characterized by classical wave theory, the r.m.s. wave-induced (or periodic) velocity components $(\overline{\tilde{u}^2})^{\frac{1}{2}}$ and $((\overline{\tilde{v}^2}))^{\frac{1}{2}}$ collapse to a single curve if the depth is normalized by $1/k$ and the velocities by $2\pi f_D\,\hat{\eta}_S/\sqrt{2}$.

5. Evidence of wave effects on the mean flow

Where waves were dominant, the mean velocity profiles have slopes different from 2.5 in the logarithmic region. Furthermore, there is a change of slope in a number of these profiles. Such behaviour is not found in typical two-dimensional boundary-layer-type flows, even under mild pressure gradients. Cheung (1984) demonstrated that the anomalous slopes are not caused by pressure gradients, the origin of the y^+ coordinate at the mean water level, potential three-dimensionality of the mean or wave flow fields, or the shift in the measured velocity caused by the mean flow following the water surface. Finally, the slope of the profile at low wind speeds is near 2.5 for the wind-wave cases and less than 2.5 for the mechanical-wave cases, while the recirculation in the tank is essentially equivalent. Thus, while recirculating flow may affect the shear-stress distribution (Wang & Wu 1985), it does not affect the slope of the velocity profile.

Consequently, it is reasonable to assert that wave dynamics are responsible for the unusual slope in the mean profiles. For $u_\infty < 3$ m/s in Case I, the u'_{rms} is always larger than $\tilde{u}_{rms}$ at all depths. At higher wind speeds, there are values of $-y^+$ at which $u'_{rms} > \tilde{u}_{rms}$ and also $u'_{rms} < \tilde{u}_{rms}$. If the waves do affect the mean profiles, then in the

region where $u'_{\rm rms} < \tilde{u}_{\rm rms}$, the mean profiles may deviate from the 2.5 slopes. On the other hand, the slopes should approach 2.5 in regions where $u'_{\rm rms} > \tilde{u}_{\rm rms}$. For Case I, it is found that in the region where $u'_{\rm rms} > 2\,(\tilde{u}_{\rm rms})$, the mean profiles have slopes nearly equal to 2.5; and where $u'_{\rm rms} < \tilde{u}_{\rm rms}$, the slopes are smaller than 2.5. Furthermore, the slopes change from 2.5 to less than 2.5 at depths where $u'_{\rm rms} \approx 2\,(\tilde{u}_{\rm rms})$, e.g. in cases with 3.2 m/s $< u_\infty <$ 9.9 m/s. These observations were derived from experiments in Case I; if these observations are the outcomes of some basic physical principles, then they should apply to Case II also. This is indeed the case. Generally $u'_{\rm rms} < \tilde{u}_{\rm rms}$ (recall that here $u' = u_{\rm R} + u_{\rm T}$ and $\tilde{u}$ represents the mechanical-wave-induced motions) in mechanical-wave experiments, and the mean profiles have slopes less than 2.5. In addition, there is no change of slope (in the logarithmic region) in the profiles for Case II, because no region exists where $u'_{\rm rms} \approx \tilde{u}_{\rm rms}$. In the light of the experimental evidence, the waves do affect the mean flow.

Shemdin (1972), Wu (1975) and Dobroklonskiy & Lesnikov (1975) reported logarithmic mean velocity profiles for their studies in which Lagrangian velocities were obtained with floats or neutrally buoyant particles. Lin & Gad-el-Hak (1984) and Wu (1975) also reported logarithmic profiles for Eulerian measurements. None of these authors reported anomalies in the profile slopes or breaks in the profiles. In the experiments of Lin & Gad-el-Hak, the short fetch might not have allowed development of wave motion sufficient to cause a slope change. In all cases there are not sufficient data to permit us to assess the potential for wave effects (as defined above) and all of the authors chose to determine the shear velocity and roughness length from the profile data, rather than having an independent measurement of shear stress as we have obtained. This required them to assume $\kappa = 0.4$, making it impossible to determine the profile slope independently. However, the Lagrangian measurements include the Stokes drift; as a result the reported mean horizontal velocities are larger than the Eulerian velocities, especially near the surface where the Stokes drift is strongest. In general the reported Lagrangian profiles possess essentially a single slope when plotted in law-of-the-wall coordinates. If the Stokes drift were removed, the profiles would have a *smaller* slope in the zone where the wave action is strongest, just as observed in our work. Thus, we are only able to conclude that the previous results are not inconsistent with our work; we can suggest that treating the velocities consistently in an Eulerian frame is preferable because it reveals the influence of the waves on the mean flow.

6. Evidence of wave-generated turbulence

In Case I, the turbulent intensity ($u'_{\rm rms}$ or $v'_{\rm rms}$) profiles are very similar to those in a steady pure-shear flow. That is, the turbulence is non-isotropic with $u'_{\rm rms} > v'_{\rm rms}$. In addition, the $\tilde{u}_{\rm rms}$ exceeds $u'_{\rm rms}$, but at most by a factor of about two. Although the wave fluctuation is strong, it remains of the same order as the turbulent motion. Also, the wave motion decays fairly rapidly with depth. On the other hand, the vertical and horizontal fluctuation intensities in Case II are almost equal in magnitude, i.e. the fluctuations (as defined by the phase-averaging process) are nearly isotropic. The $\tilde{u}_{\rm rms}$ now exceeds $u'_{\rm rms}$ by more than a factor of two, attaining a value of 10 in low-wind-speed experiments when mechanical waves were dominant. The decay of the wave motion with depth is not as rapid as that in Case I because the mechanical waves have a greater wavelength. Thus, if there is wave-generated turbulence, the phenomenon ought to be more prominent in the mechanical-wave experiments.

The apparent deviation of the fluctuation intensities in Cases II from those of the wind-wave experiments (cf. figures 2 and 6) leads us to ask why the $u'_{\rm rms}$ and $v'_{\rm rms}$ profiles behave quite differently in cases I and II? For Case II, we decomposed u' as

$$u' = u_{\rm R} + u_{\rm T}, \tag{6}$$

where $u_{\rm R}$ is the velocity fluctuation induced by wind-generated ripples, and $u_{\rm T}$ is the velocity fluctuation presumed to be caused by turbulent motions. Then,

$$\overline{u'^2} = \overline{u_{\rm R}^2} + \overline{u_{\rm T}^2} + 2\overline{u_{\rm R}\,u_{\rm T}}, \tag{7}$$

$$\overline{u'v'} = \overline{u_{\rm T}\,v_{\rm T}} + \overline{u_{\rm T}\,v_{\rm R}} + \overline{u_{\rm R}\,v_{\rm T}} + \overline{u_{\rm R}\,v_{\rm R}}. \tag{8}$$

The ripple-induced velocities $u_{\rm R}$ and $v_{\rm R}$ are caused by small wind-generated water waves. Thus, their correlations with $u_{\rm T}$ and $v_{\rm T}$ should be small (as in the Case I experiments). Further, $u_{\rm R}$ and $v_{\rm R}$ must be nearly 90° out of phase. Therefore, we conclude that

$$\overline{u'^2} = \overline{u_{\rm R}^2} + \overline{u_{\rm T}^2} \quad \text{or} \quad (\overline{u'^2})^{\frac{1}{2}} = (\overline{u_{\rm R}^2} + \overline{u_{\rm T}^2})^{\frac{1}{2}} \tag{9}$$

and

$$\overline{u'v'} = \overline{u'_{\rm T}\,v'_{\rm T}}. \tag{10}$$

Then, the definitions of the friction velocity (u_*) and the turbulent boundary-layer thickness (δ) are consistent with those in the wind-wave experiments because $\overline{u'v'}$ is not strongly affected by the ripple-induced velocities.

As noted in §2, we can calculate $\eta_{\rm R}$ by subtracting the phase-averaged results from the raw data. Furthermore, by assuming the ripples also obey linear water-wave theory, we can estimate the ripple-induced velocity from (4) by using the ripple spectrum $S_{\eta_{\rm R}\eta_{\rm R}}(f)$ instead of the total wave-height spectrum (see Cheung 1984). Using this method, we obtain $\overline{u_{\rm R}^2}$. Then, from (9),

$$\overline{u_{\rm T}^2} = \overline{u'^2} - \overline{u_{\rm R}^2}. \tag{11}$$

The results for the horizontal velocities are shown in figures 6 (u'), 7 ($u_{\rm R}$) and 8 ($u_{\rm T}$). Although the ripple-induced velocities are not expected to scale well when normalized by u_* and plotted versus $-y/\delta$, we do that here to illustrate that they are small and that $\overline{u'^2}$ is dominated by the purely turbulent fluctuations (cf. figures 6 and 8). The crucial result follows from a comparison of figures 2 and 8. For the wind waves Case I (figure 2), the turbulent fluctuations are not distinguishable from those found in a solid-wall boundary layer. However, in the mechanically generated waves, Case II, there is a marked increase in the turbulence level. This suggests that mechanically generated waves are able to transfer energy to the turbulence field in the region where the waves are energetic, the decay of the turbulent r.m.s. with depth following closely the decay of the wave r.m.s. velocities.

Finally, if the waves are truly irrotational, the mean wave-induced shear stress ($-\overline{\tilde{u}\,\tilde{v}}$) should be zero, and the wave field should not interact with either the mean or the turbulent flow fields. It is clear from the data that the waves are not truly irrotational. This agrees with the field data of Shonting (1964, 1967, 1968, 1970), Yefimov & Kristoforov (1969, 1971), Cavaleri *et al.* (1978), as well as the laboratory results of Howe *et al.* (1981). They all found that the vertical and horizontal velocities were not in quadrature. If they are not, the mean wave-induced shear stress must be non-zero. Consequently, this shear stress may contribute to turbulence production directly or indirectly. The mean wave-induced shear stress is much larger in Case II than in Case I. This result again implies that the effect of the mean wave-induced shear stress is stronger in mechanical-wave experiments (cf. Jones & Kenney 1977,

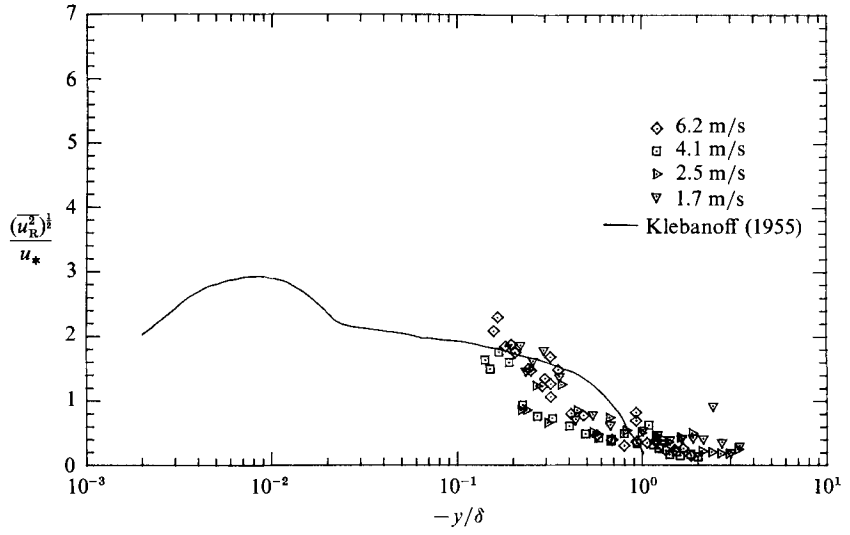

FIGURE 7. $(\overline{u_R^2})^{\frac{1}{2}}/u_*$ versus $-y/\delta$: mechanical waves (case II).

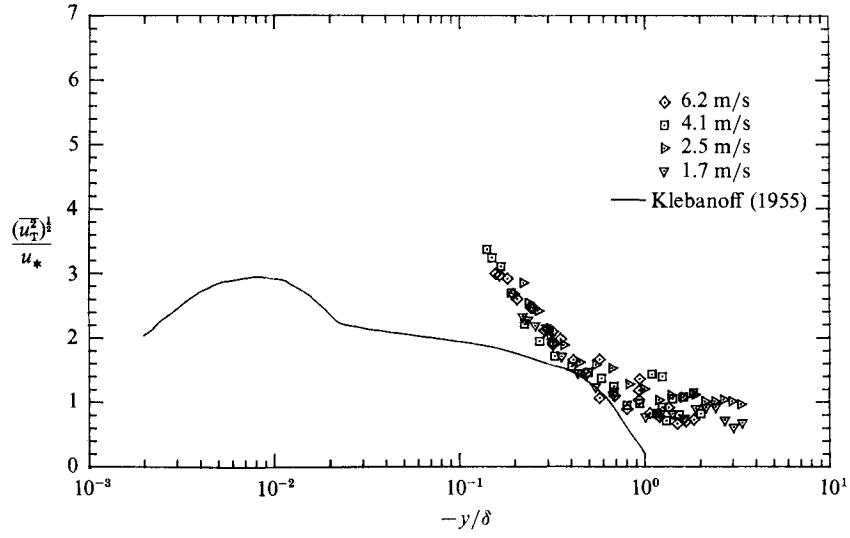

FIGURE 8. $(\overline{u_T^2})^{\frac{1}{2}}/u_*$ versus $-y/\delta$: mechanical waves (case II).

who concluded, from analysis of wind-wave data from aquatic mixed layers in field experiments, that the surface-wave orbital velocities act merely as 'inactive' motions and do not interfere with low-frequency stress-carrying eddies).

Our experimental data support the postulate that the waves can affect the mean flow. It is well known that turbulence can only be maintained by drawing energy from the mean flow or, as suggested above, from the waves as well. Hence, the mean, wave and turbulent fields are closely coupled. Although the experimental evidence for such coupling is strong (e.g. Bliven *et al.* 1984 showed the existence of a Reynolds stress that increased as the wave steepness increased and decayed exponentially with depth), it is crucial to demonstrate, from a theoretical viewpoint, that the governing equations allow such interactions.

7. Analysis of the governing equations: energy transfer estimates

Based on the characteristic scales for different parts of the flows, an order-of-magnitude analysis can be performed on the terms in the governing equations. A detailed description of such an analysis is given in Cheung (1984). Here, we present only the results of the analysis of the kinetic-energy equations because, while analysis of the momentum equations shows that coupling exists among the mean, wave and turbulent fields, the interaction among the three fields is best illustrated by the energy equations. The kinetic-energy equations can be obtained from the momentum equations as shown by Reynolds & Hussain (1972). There are three terms of interest, namely,

$$\underset{\text{I}}{(-\overline{\tilde{u}_i\tilde{u}_j})\frac{\partial\bar{u}_i}{\partial x_j}}, \quad \underset{\text{II}}{(-\overline{u_i'u_j'})\frac{\partial\bar{u}_i}{\partial x_j}}, \quad \underset{\text{III}}{-\overline{\langle u_i'u_j'\rangle\frac{\partial\tilde{u}_i}{\partial x_j}}}.$$

Term I, when it is positive, represents the production of the wave kinetic energy by the mean wave-induced stresses $-\overline{\tilde{u}_i\tilde{u}_j}$. The same term appears with an opposite sign in the equation for wave kinetic energy. Similarly, Term II represents the production of the turbulent kinetic energy by the mean Reynolds stresses $-\overline{u_i'u_j'}$. This term shows up as an energy source term in the equation for turbulent kinetic energy. Term III represents turbulent energy production by the waves via the action of the phase-averaged turbulent Reynolds stresses $-\langle u_i'u_j'\rangle = -\overline{u_i'u_j'} - \tilde{r}_{ij}$. This term can also be rewritten as $-\overline{\tilde{r}_{ij}(\partial\tilde{u}_i/\partial x_j)}$. It is present in the energy equations for both the wave and turbulence, but with opposite signs.

Terms I, II and III clearly show the interaction among the mean, wave and turbulent fields. Term I denotes a summation of 9 terms, among which $-\overline{\tilde{u}\tilde{v}}\,(\partial\bar{u}/\partial y)$ is dominant. The mean velocity gradient $\partial\bar{u}/\partial y$ is positive in Cases I and II, and $-\overline{\tilde{u}\tilde{v}}$ is generally negative. Thus, the wave production term is negative; in other words, energy is transferred from the wave field to the mean field. Hussain (1983) suggested that negative production is a simple consequence of coherent structures in turbulent shear flows. However, whether or not the wave-induced motions can be classified as coherent structures is unimportant; we note only that negative production from organized flow structures is not an uncommon phenomenon. The production term was found to be increasingly negative near the interface and to decay (become less negative) rapidly with depth, since both $-\overline{\tilde{u}\tilde{v}}$ and $\partial\bar{u}/\partial y$ diminish away from the interface. Some typical profiles of this production term are shown in figure 9 for Case II, where the effect is most pronounced.

It is obvious that the mean and wave fields in the water both draw energy directly from the wind. The energy production or dissipation terms from the energy equations indicate here only the direction of transfer within the water layer. In particular, the negative production of the waves means that they also increase the kinetic energy of the mean flow.

Turbulence seems to draw its energy from the mean field through Term II or from the wave field through Term III. The dominant component in Term II is $-\overline{u'v'}(\partial\bar{u}/\partial y)$, and it is always positive in the experiments. Thus, energy is drained from the mean field to the turbulent field. In wind-wave experiments, the turbulence production (Term II) is larger than the wave production (Term I) at all wind speeds, even though in some cases both terms are about the same order of magnitude near the interface. On the other hand, the magnitude of the wave-production term is greater than that of the turbulence-production term in the mechanical-wave experiments.

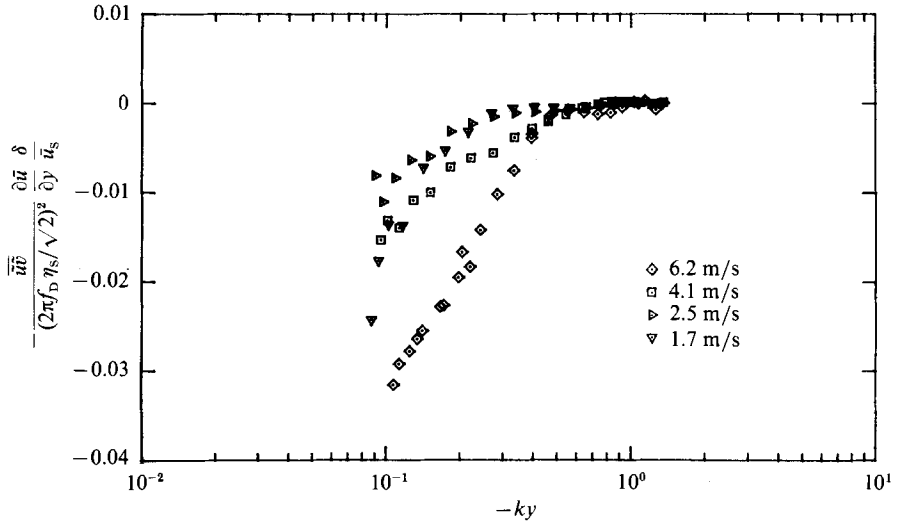

FIGURE 9. $-\overline{\tilde{u}\tilde{v}}\,\partial\bar{u}/\partial y$ profiles in dimensionless units: mechanical waves (case II).

Thus, in the Case I experiments the sum of Terms I and II is *positive* in the mean kinetic-energy equation. Accordingly, the net effect of the two production terms is similar to the turbulence production term in a pure shear flow – a net drain of energy from the mean flow. This may be the reason why, in the wind-wave, Case I, the turbulent intensities ($u'_{\rm rms}$ and $v'_{\rm rms}$) have trends similar to those for flows over flat plates. However, the net production is *negative* in mechanical-wave experiments – a result which may explain the unusual trends of the turbulent intensities for mechanical-wave experiments.

There are four dominant components in Term III, namely,

$$-\overline{\tilde{r}_{11}\frac{\partial\tilde{u}}{\partial x}},\quad -\overline{\tilde{r}_{12}\frac{\partial\tilde{u}}{\partial y}},\quad -\overline{\tilde{r}_{12}\frac{\partial\tilde{v}}{\partial x}},\quad -\overline{\tilde{r}_{22}\frac{\partial\tilde{v}}{\partial y}}.$$

If we assume that

$$\tilde{u}_i = \hat{u}_i\cos(kx-\omega t-\theta_{u_i}),$$

$$\frac{\partial\tilde{u}_i}{\partial y} = k\tilde{u}_i,$$

$$\tilde{r}_{ij} = \hat{r}_{ij}\cos(kx-\omega t-\theta_{\tilde{r}_{ij}}),$$

then the components in Term III can be found from the data. However, in fixed-frame experiments, there is much uncertainty in $\theta_{\tilde{r}_{ij}}$. The uncertainty is not due to instrumentation but to kinematics. All $\theta_{\tilde{r}_{ij}}$ seem to have a value near 180° relative to $\tilde{\eta}$. The measurements were made in a fixed frame and the probe was closest to the interface at the wave trough, which is the 180° phase-angle point of $\tilde{\eta}$. Consequently, since the $\tilde{r}_{ij}$ are expected to be higher near the interface, the phase angles of $\tilde{r}_{ij}$ may be due to kinematics of the waves and not due to the dynamics. The effects of the wavy motion may not be as severe at deeper depths and the $\theta_{\tilde{r}_{ij}}$ may indeed be the true phase angles, but at large depths ($\sim 1/k$) Term III is most likely negligible. Thus, we were unable to draw any useful conclusions about the components of Term III from these fixed-frame measurements.

8. Conclusions

In this study we developed a comprehensive data set on momentum transfer at an air–water interface under a range of surface conditions (see Cheung 1984). The data set should prove very useful in evaluating current or future computational schemes as well as turbulence models for air–sea interaction.

When the flow field beneath the air–water interface is separated into mean, wave and turbulent components, each can be characterized by significant velocity and length scales (see table 1). Our work is the first verification of the relevance of these scales although many have been suggested by other investigators, e.g. Navrotskii (1967) and Kitaigorodskii *et al.* (1983). The absolute magnitudes of these scales are not as important as their relative magnitudes. In the wind-wave experiments y_η is always much smaller than δ, but in all mechanical-wave experiments δ is always less than $1/k \approx y_\eta$. The boundary-layer thickness δ is larger in the wind-wave cases than in the mechanical-wave cases at comparable wind speeds, possibly due to the reduced drift velocity in the latter case (see §4). However, the friction velocities remain of the same order of magnitude at equivalent wind speeds, regardless of surface conditions. Of course, $1/k$ and all values of y_η and δ are small compared to the fetch of 13 m.

A simple analysis of the governing equations using the experimentally obtained characteristic scales shows that there are interactions among the mean, wave and turbulent fields. The wave field affects the mean flow directly, which leads to a change in slope in the steady form of the law of the wall, although the logarithmic region persists in the velocity profiles. Moreover, the kinetic energy of the mean flow is augmented by the presence of waves. Turbulence draws its energy mainly from the mean flow, but the turbulence can be augmented by the waves because the waves affect the mean flow. However, the turbulent-intensity profiles in wind-wave experiments are similar to those for flows over flat plates, but the profiles in mechanical-wave experiments are very different. This result suggests a coupling between turbulence and motions induced by mechanically generated waves.

The research was carried out under Contract N00014-84-0242, NR-661-003/11-18/83 (430) from the Mechanics Division, Office of Naval Research. Initial studies were made under NSF Grant ENG-79-01176. The authors are indebted to Ms Jih-Yih Jiang for computing the ripple-induced velocities for the mechanically generated wave data sets and to our colleague Dr Stephen Klotz for his review of the manuscript and many useful suggestions.

REFERENCES

Benilov, A. Yu., Kouznetsov, O. A. & Panin, G. N. 1974 On the analysis of wind wave-induced disturbances in the atmospheric turbulent surface layer. *Boundary-Layer Met.* **6**, 269–285.

Bliven, L. F., Huang, N. E. & Long, S. R. 1984 A laboratory study of the velocity field below surface gravity waves. In *Gas Transfer at Water Surfaces* (ed. W. Brutsaert & G. H. Jirka), pp. 181–190. Reidel.

Bole, J. B. & Hsu, E. Y. 1969 Response of gravity water waves to wind excitation. *J. Fluid Mech.* **35**, 657–675.

Bowden, K. F. & White, R. A. 1966 Measurements of the orbital velocities of sea waves and their use in determining the directional spectrum. *Geophys. J. R. Astron. Soc.* **12**, 33–54.

Bye, J. A. T. 1967 The wave-drift current. *J. Mar. Res.* **25**, 95–102.

Cavaleri, O., Ewing, J. A. & Smith, N. D. 1978 Measurement of the pressure and velocity field below surface waves. In *Turbulent Fluxes Through the Sea Surface, Wave Dynamics, and Prediction* (ed. A. Favre & K. Hasselmann), pp. 257–272. Plenum.

CHEUNG, T. K. 1984 A study of the turbulent layer in the water at an air–water interface. Ph.D. dissertation, Dept. of Civil Engineering, Stanford University (also available as *Tech. Rep.* 287, 1985).

DOBROKLONSKIY, S. V. & LESNIKOV, B. M. 1975 A laboratory study of the dynamic characteristics of drift currents in the presence of wind-driven waves. *Izv. Akad. Nauk. SSSR Atmos. Ocean. Phys.* **11**, 590–595.

DONELAN, M. A. 1978 Whitecaps and momentum transfer. In *Turbulent Fluxes Through the Sea Surface, Wave Dynamics, and Prediction* (ed. A. Favre & K. Hasselmann), pp. 273–288. Plenum.

GOOSSENS, L. H. J., VAN PAGEE, H. J. A. & TESSEL, P. J. 1982 Vertical turbulent diffusion in air-driven water flows. *J. Hydraul. Div., ASCE* **108**, 995–1009.

HOWE, B. M., CHAMBERS, A. J., KLOTZ, S. P., CHEUNG, T. K. & STREET, R. L. 1981 A preliminary report on velocity and temperature measurements above and beneath an air–water interface: the data set. *Stanford University, Dept Civil Eng., Tech. Rep.* 261.

HOWE, B. M., CHAMBERS, A. J., KLOTZ, S. P., CHEUNG, T. K. & STREET, R. L. 1982 Comparison of profiles and fluxes of heat and momentum above and below an air–water interface. *Trans. ASME* C: *J. Heat Transfer* **104**, 34–39.

HSU, C. T., HSU, E. Y. & STREET, R. L. 1981 On the structure of turbulent flow over a progressive water wave: theory and experiment in a transformed, wave-following coordinate system. *J. Fluid Mech.* **105**, 87–117.

HUSSAIN, A. K. M. F. 1983 Coherent structures – reality and myth. *Phys. Fluids* **26**, 2816–2850.

HUSSAIN, A. K. M. F. & REYNOLDS, W. C. 1970 The mechanics of an organized wave in turbulent shear flow. *J. Fluid Mech.* **41**, 241–258.

JONES, I. S. F. & KENNEY, B. C. 1977 The scaling of velocity fluctuations in the surface mixed layer. *J. Geophys. Res.* **82**, 1392–1396.

KITAIGORODSKII, S. A., DONELAN, M. A., LUMLEY, J. L. & TERRAY, E. A. 1983 Wave–turbulence interactions in the upper ocean. Part II: Statistical characteristics of wave and turbulent components of the random velocity field in the marine surface layer. *J. Phys. Oceanogr.* **13**, 1988–1999.

KLEBANOFF, P. S. 1955 Characteristics of turbulence in a boundary layer flow with zero pressure gradient. *NACA Rep.* 1247.

KLINE, S. J. & MCCLINTOCK, F. A. 1953 Describing uncertainties in single-sample experiments. *Mech. Engng* **75**, 3–8.

KONDO, J. 1976 Parameterization of turbulent transport in the top meter of the ocean. *J. Phys. Oceanogr.* **6**, 712–720.

LIN, J. & GAD-EL-HAK, M. 1984 Turbulent current measurements in a wind-wave tank. *J. Geophys. Res.* **89**, 627–636.

MCLEISH, W. L. & PUTLAND, G. E. 1975 Measurements of wind-driven flow profiles in the top millimeter of water. *J. Phys. Oceanogr.* **5**, 516–518.

MOFFAT, R. J. 1981 Contribution to the theory of uncertainty analysis for single-sample experiments, Vol. I. *The 1980–81 AFOSR-HTTM-Stanford Conference on Complex Turbulent Flows.* Stanford University Dept. Mech. Eng., Thermoscience Div.

NAVROTSKII, V. V. 1967 Waves and turbulence in the ocean surface layer. *Oceanology, Akad. Nauk. SSSR* **7**, 755–766.

PHILLIPS, O. M. 1977 *The Dynamics of the Upper Ocean*, 2nd edn. Cambridge University Press.

PHILLIPS, O. M. & BANNER, M. L. 1974 Wave breaking in the presence of wind drift and swell. *J. Fluid Mech.* **66**, 625–640.

REYNOLDS, W. C. & HUSSAIN, A. K. M. F. 1972 The mechanics of an organized wave in turbulent shear flow. Part 3. Theoretical models and comparisons with experiments. *J. Fluid Mech.* **54**, 263–288.

SCHLICHTING, H. 1979 *Boundary-Layer Theory*, 7th edn. McGraw-Hill.

SHEMDIN, O. H. 1972 Wind-generated current and phase speed of wind waves. *J. Phys. Oceanogr.* **2**, 411–419.

SHONTING, D. H. 1964 A preliminary investigation of momentum flux in ocean waves. *Pure Appl. Geophys.* **57**, 149–152.

SHONTING, D. H. 1967 Measurements of particle motions in ocean waves. *J. Mar. Res.* **25**, 162–181.

SHONTING, D. H. 1968 Autospectra of observed particle motion in wind waves. *J. Mar. Res.* **26**, 411–419.

SHONTING, D. H. 1970 Observations of Reynolds stresses in wind waves. *Pure Appl. Geophys.* **81**, 202–210.

SIMPSON, J. H. 1969 Observations of the directional characteristics of sea waves. *Geophys. J. R. Astron. Soc.* **17**, 93–120.

TAIRA, K. 1971 Wave particle velocities measured with a Doppler current meter. *J. Ocean. Soc. Japan* **27**, 218–232.

TAKEUCHI, K. & MOGEL, T. R. 1975 A performance of a mini-computer. *Rev. Scient. Instrum.* **46**, 686–691.

TENNEKES, H. & LUMLEY, J. L. 1972 *A First Course in Turbulence.* MIT Press.

THORNTON, E. B. & KRAPOHL, R. F. 1974 Water particle velocities measured under ocean waves. *J. Geophys. Res.* **79**, 847–852.

WANG, J. & WU, J. 1985 Wind-induced water turbulence. *The Ocean Surface*, pp. 401–406. Reidel.

WU, J. 1968 Laboratory studies of wind-wave interactions. *J. Fluid Mech.* **34**, 91–111.

WU, J. 1975 Wind-induced drift currents. *J. Fluid Mech.* **68**, 49–70.

YEFIMOV, V. V. & KHRISTOFOROV, G. N. 1969 Some features of the velocity field in the layer of wind-driven swell. *Izv. Akad. Nauk. SSSR, Atmos. Ocean. Phys.* **5**, 597–602.

YEFIMOV, V. V. & KHRISTOFOROV, G. N. 1971 Spectra and statistical relations between the velocity fluctuations in the upper layer of the seas and surface waves. *Izv. Akad. Nauk. SSSR, Atmos. Ocean. Phys.* **7**, 841–851.